Nonlinear electromagnetic fields in 0.5 MHz inductively coupled plasmas

K. Ostrikov[a)]
School of Chemistry, Physics and Earth Sciences, The Flinders University of South Australia, GPO Box 2100, Adelaide SA 5001, Australia
and Plasmas Sources and Applications Center, NIE, Nanyang Technological University, 1 Nanyang Walk, 637616 Singapore

E. Tsakadze
Plasmas Sources and Applications Center, NIE, Nanyang Technological University, 1 Nanyang Walk, 637616 Singapore
and Optics and Fluid Dynamics Department, RISOE National Laboratory, P.O. Box 49, DK-4000 Roskilde, Denmark

S. Xu
Plasmas Sources and Applications Center, NIE, Nanyang Technological University, 1 Nanyang Walk, 637616 Singapore

S. V. Vladimirov
Department of Theoretical Physics, School of Physics, The University of Sydney, New South Wales 2006, Australia

R. Storer
School of Chemistry, Physics and Earth Sciences, The Flinders University of South Australia, GPO Box 2100, Adelaide SA 5001, Australia

(Received 26 November 2002; accepted 16 December 2002)

Radial profiles of magnetic fields in the electrostatic (E) and electromagnetic (H) modes of low-frequency ($\sim$500 kHz) inductively coupled plasmas have been measured using miniature magnetic probes. In the low-power ($\sim$170 W) E-mode, the magnetic field pattern is purely linear, with the fundamental frequency harmonics only. After transition to higher-power ($\sim$1130 W) H-mode, the second-harmonic nonlinear azimuthal magnetic field $B_\phi^{2\omega}$ that is in 4–6 times larger than the fundamental frequency component B_ϕ^{ω}, has been observed. A simplified plasma fluid model explaining the generation of the second harmonics of the azimuthal magnetic field in the plasma source is proposed. The nonlinear second harmonic poloidal ($r-z$) rf current generating the azimuthal magnetic field $B_\phi^{2\omega}$ is attributed to nonlinear interactions between the fundamental frequency radial and axial magnetic fields with the azimuthal rf current. © *2003 American Institute of Physics.* [DOI: 10.1063/1.1557871]

I. INTRODUCTION

Low-pressure, low-temperature inductively coupled plasma (ICP) sources have been currently adopted by a number of high-tech industries as reference plasma reactors for numerous applications in microelectronics, materials synthesis, and processing.[1] Recently, the ICPs have proved instrumental in various nanoscale processes, including but not limited to, nanostructuring surfaces and interfaces, growth of nanoscaled objects with various organizations and architectures, such as nanoparticles, nanorods, nanotubes, and several others.[2]

One of the most common ICP-generating discharge configurations includes an external flat spiral (commonly known as a ''pancake'') inductive coil placed externally to a dielectric-sealed metal vacuum chamber and delivering rf power to the plasma being created.[3–5] In a common cylindrical embodiment with a dielectric window atop (in $r-\phi$ cross-section), similar to what has been used in our experiments (Fig. 1), a rf current spirally-driven in the coil predominantly excites the azimuthal rf electric field, as well as poloidal (with B_z and B_r components) magnetic field.[6] Generation of the above currents and electromagnetic fields have been extensively confirmed by numerous modeling and simulation results[7–11] within the framework of the linear, with respect to the rf field amplitude, approximation, which is normally valid at low rf input powers.

However, the linear approximation can often be inconsistent even at low powers, e.g., in a low-frequency operation regime. Indeed, a parameter of nonlinearity, which is a ratio of the electron quiver velocity $V_E=eE/m_e\omega$ in rf electric field E of frequency ω to the electron thermal velocity V_{Te}, increases approximately 27 times when the operating frequency is decreased from the conventional one 13.56 MHz to 500 kHz. Furthermore, operating ICPs at lower frequencies has provided a number of indisputable advantages, such as weak capacitive coupling, redundancy of any electrostatic shield of the inductive coil, excellent uniformity of major

a)Author to whom correspondence should be addressed. Electronic mail: kostrikov@nie.edu.sg

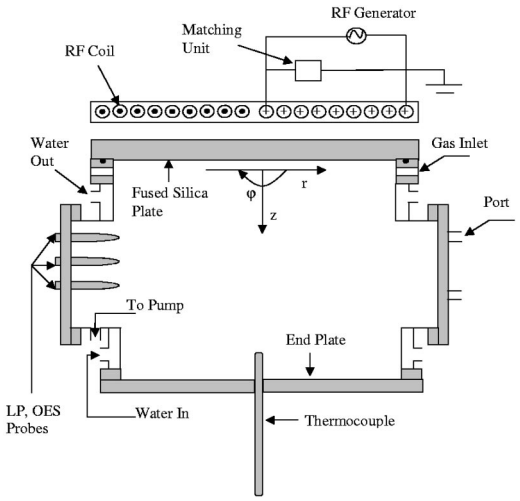

FIG. 1. Schematic diagram of the plasma source.

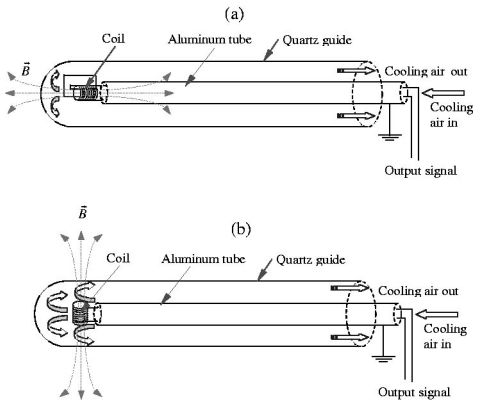

FIG. 2. Schematics of miniature magnetic probes for radial (a), axial and azimuthal (b), magnetic field components.

plasma parameters over large areas and volumes, and several others.[12–14]

Hence, at low frequencies, one should expect significant distortions of the electromagnetic field/current patterns, which can be due to the generation of nonlinear signals at higher Fourier harmonics or static nonlinear (ponderomotive) responses. Hysteretic effects in mode transition phenomena is yet another intrinsically nonlinear feature of inductively coupled plasmas.[5,13]

Here, we investigate distribution of nonlinear electromagnetic fields in a low-frequency (500 kHz) source of inductively coupled plasmas. We also show that the nonlinear plasma response results in generation of the azimuthal magnetic field component, which does not appear in the linear regime at lower rf powers. A theoretical explanation of the persistent nonlinear second-harmonic signal is provided.

II. EXPERIMENT

Schematics of the low-frequency inductively coupled plasma source, with the coordinates used, is given in Fig. 1. A vacuum vessel is a double-walled, water-chilled stainless steel chamber, with the inner radius of $R=16$ cm and length of $L=20$ cm. A vacuum-tight 12 mm thick quartz window seals off the chamber from the top. Four rectangular side ports with seven axially aligned portholes have been designed to enable access of various diagnostic tools, such as Langmuir and magnetic probes into the chamber. The vacuum system comprises a $450\,\mathrm{l\,s^{-1}}$ turbomolecular pump backed by a two-stage rotary pump and allows one to achieve typical base pressures of $\sim 10^{-5}$ Torr. The inflow rate and pressure of the working gas can be controlled by a combination of a gate valve and MKS mass-flow controllers. In our experiments, the gas feedstock pressure p_0 was maintained in the range of 10–100 mTorr. However, the plasma source is capable for stable work within the pressure range of 0.3–1000 mTorr (Ref. 13) peculiar for most of the plasma processing applications.[15] The rf power is deposited onto the chamber volume via a 17-turn flat spiral (''pancake''), water-chilled coil, separated from the top of the quartz window by a small, 3 mm air gap. A low frequency ($\sim$500 kHz) rf generator is connected to the coil via a π-type matching network.

The rf magnetic fields generated in the vacuum chamber have been measured using two miniature magnetic probes (Fig. 2). Each of the probes was made of 5 mm thick cylindrical Teflon heads mounted on thinner hollow aluminum tubes with insulated copper wires inside. The wires were wound over the probe surface to form miniature (20–25 turn) solenoids oriented as shown in Fig. 2. One of the probes can sense the radial magnetic field component [B_r, Fig. 2(a)], while the other one, being properly oriented, measures either B_ϕ or B_z components [Fig. 2(b)]. The probes have been inserted radially through the portholes in the diagnostic side port of the chamber. Afterwards, rf signals collected by the probes were processed by the data acquisition system and further deconvoluted into fundamental, first, second, and third Fourier harmonics.

The radial distribution of the magnetic fields in the chamber was investigated separately in the electrostatic (E) and electromagnetic (H) discharge regimes by sweeping the probes radially inside a quartz tube inserted through the closest to the quartz window porthole ($z=4$ cm). In the electrostatic discharge mode sustained with low ($\sim$170 W) rf powers, the electromagnetic field pattern includes all three components of the rf magnetic field, namely B_r, B_ϕ, and B_z (Fig. 3). Apparently, the field pattern features only the fundamental frequency signals. Specifically, the second harmonic signals appear to be typically 10–100 times weaker than the fundamental frequency ones. Furthermore, in the areas close to the chamber center, the B_z component is a dominant one, whereas at distances $\sim$8 cm apart from the walls, B_r becomes more pronounced. The azimuthal magnetic field component, although non-negligible, appears to be much smaller than the other two components. It is remarkable that in the low-power case the electromagnetic field pattern is consistent with the theoretical results of El-Fayoumi and Jones.[16] However, in the linear (with respect to the field amplitudes) theory that also approximates the real flat spiral inductive coil by the set of concentrical azimuthal rf currents, B_ϕ component does not persist. Nevertheless, since no other Fourier harmonics were detected in the E-mode dis-

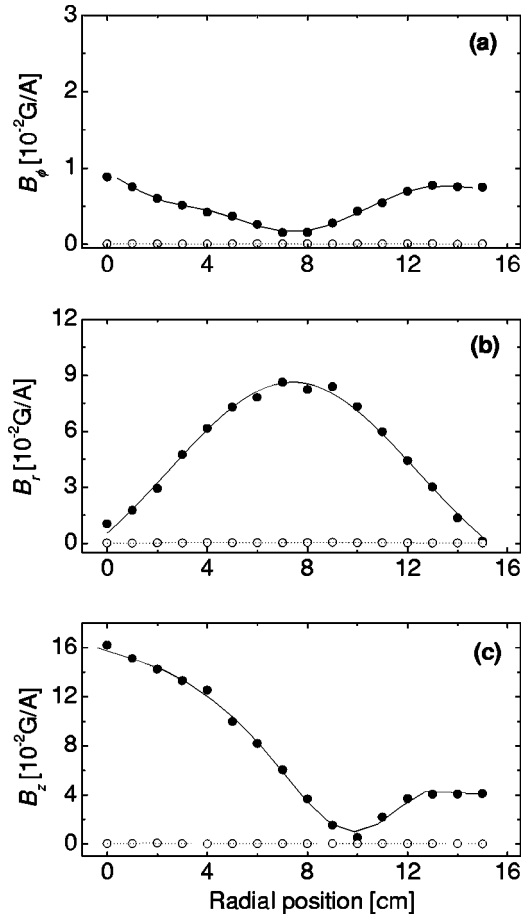

FIG. 3. Radial profiles of B_ϕ (a), B_r (b), and B_z (c) components in the E-mode discharge sustained with 170 W rf powers at 50.8 mTorr. Solid and open circles correspond to the fundamental frequency and second harmonic signals, respectively.

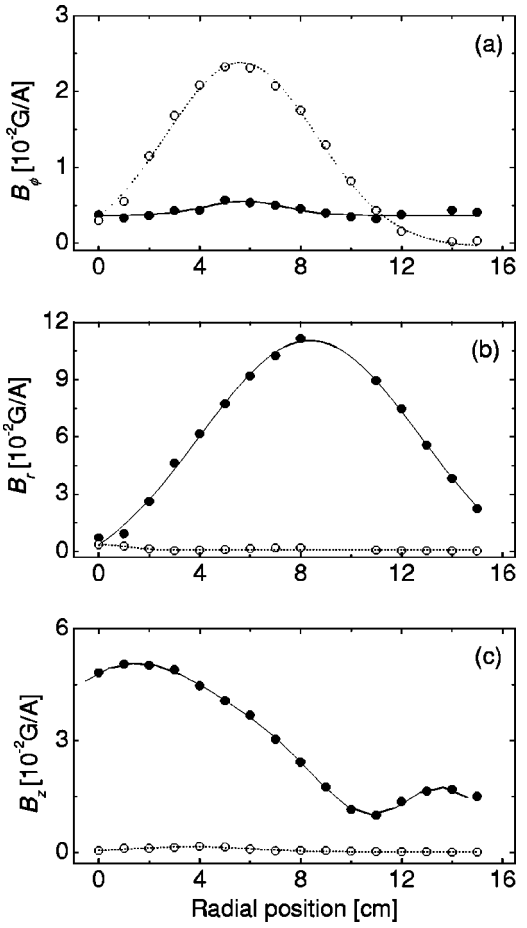

FIG. 4. Same as in Fig. 3 for the H-mode discharge at $P_{\text{in}}=1130$ W.

charge, the measured azimuthal magnetic field signal can be attributed to nonvanishing radial rf electric field generated by the real planar spiral coil. Thus, we note that the nonlinear effects are negligible in the low-power electrostatic regime.

After transition to the electromagnetic mode, the field pattern changes dramatically (Fig. 4). In particular, the fundamental component of B_z becomes even smaller than in the E-mode discharge. More importantly, a pronounced generation of the second Fourier harmonics of B_ϕ was clearly observed [Fig. 4(a)]. It is remarkable that the amplitude of the second-harmonic nonlinear signal $|B_\phi^{2\omega}|$ appears to be 4–6 times higher than that of the fundamental harmonics. The maximum of the amplitude of the second Fourier harmonic is located at approximately 5–6 cm from the chamber axis. It has also been observed that the magnitude of the nonlinear magnetic field increases with rf power. It is thus reasonable to presume that the observed effect is due to the nonlinear plasma response, which normally increases with the amplitude of the fundamental harmonics.

Non-negligible second harmonic signals also appear for B_r and B_z components. However, they are much smaller than the second Fourier component of B_ϕ. Likewise, higher than the second Fourier harmonics do not affect the electromagnetic field profiles. It is worthwhile to note that the resulting magnetic field in the electromagnetic mode has a linear (fundamental frequency) poloidal $(r-z)$ component and a nonlinear (second harmonic) azimuthal component. Thus, the dominant linear rf current features a predominant azimuthal component j_ϕ, whereas the nonlinear rf current mostly flows in the poloidal cross section. This conclusion will further be elucidated theoretically below.

However, linear magnetic field components feature hysteretic effects (different behavior for increasing and decreasing rf power), as depicted in Fig. 5. In particular, when the power increases, the linear B_ϕ component increases slowly [Fig. 5(a)]. However, when the input power goes down, the latter decreases faster to smaller, than original values. The second harmonics of B_ϕ also features a hysteretic behavior. However, in contrast to the linear component, the nonlinear signal exceeds the original values in the E-mode while the power input diminishes. One can also note that the hysteretic effects for the $B_\phi^{2\omega}$ signal are less resolved in the H-mode than in the E-mode. The third Fourier harmonics appears too weak to be of any concern and is not depicted. As Figs. 5(b) and 5(c) show, the hysteretic effects are also pertinent to the purely linear B_r and B_z components. In the H-mode, the corresponding values are quite reproducible in the H-mode at increasing and decreasing powers. On the other hand, the field values in the E-mode appear to be noticeably lower when the input power is decreasing [Figs. 5(b) and 5(c)].

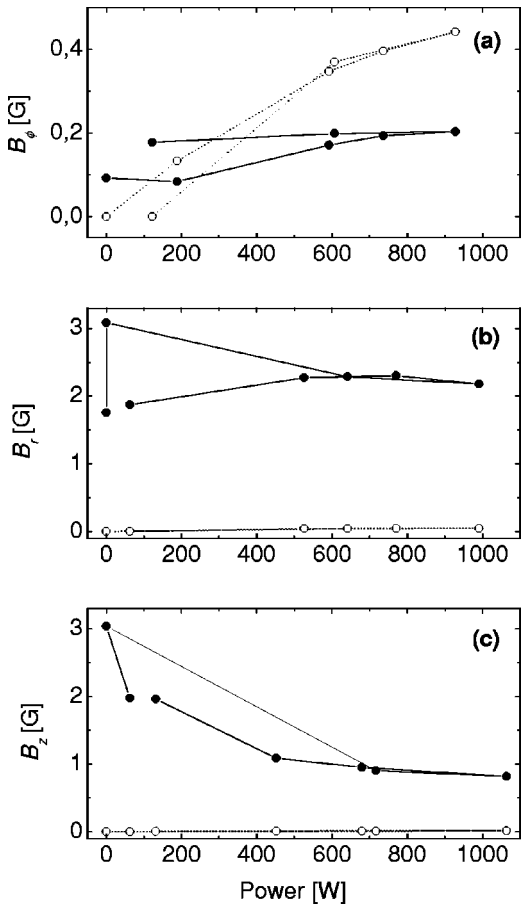

FIG. 5. Hysteresis of B_ϕ (a), B_r (b), and B_z (c) components at $p_0 = 50.8$ mTorr.

Thus, both the linear and nonlinear components of the magnetic field vary in a hysteretic (essentially nonlinear) manner during the process of $E-H-E$ mode transition.

III. FLUID MODEL

Now, using a simple fluid model, we investigate the possible reasons for the nonlinear plasma response in our experiment. In the model, only nonlinear current effects will be accounted, whereas any nonlinearities associated with pressure gradient forces will be sidestepped. Thus, assuming $T_e, n_e = \text{const}(r,\phi,z)$ (which is fairly correct at $z=4$ cm for $r<10$ cm in the H-mode discharge[13]), from the electron momentum equation

$$m_e \partial_t \mathbf{v}_e + m_e \nu_e \mathbf{v}_e + e\mathbf{E} = \mathbf{F}_{\mathrm{NL}}, \tag{1}$$

we can estimate the direction of the nonlinear force $\mathbf{F}_{\mathrm{NL}} = -m_e[(\mathbf{v}_e\nabla)\mathbf{v}_e + (e/m_e c)\mathbf{v}_e \times \mathbf{B}]$ and relevant nonlinear currents $\mathbf{j}_{\mathrm{NL}}$ resulting in the observed nonlinear second-harmonic response, where $\mathbf{E}$, $\mathbf{B}$ are the rf electric and magnetic fields. Here, $\mathbf{v}_e$, ν_e, e, and m_e are the electron fluid velocity, effective collision frequency, charge, and mass, respectively.

Expanding all the time-varying quantities in series

$$G = G_0 + (1/2)[G_1 \exp(-i\omega t) + G_2 \exp(-2i\omega t) + \cdots + \text{c.c.}],$$

where G is either of $\mathbf{v}_e$, $\mathbf{E}$, or $\mathbf{B}$, and c.c. stands for complex conjugate, we obtain

$$\mathbf{F}_{\mathrm{NL}}^{(2\omega)} = -\tfrac{1}{4}\left[m_e(\mathbf{v}_{e1}\nabla)\mathbf{v}_{e1} + \frac{e}{c}\mathbf{v}_{e1}\times\mathbf{B}_1 \right] \exp(-2i\omega t) \tag{2}$$

for the nonlinear force at the second harmonics and

$$\mathbf{F}_{\mathrm{NL}}^{(0)} = -\tfrac{1}{4}\left\{ m_e[(\mathbf{v}_{e1}^*\nabla)\mathbf{v}_{e1} + (\mathbf{v}_{e1}\nabla)\mathbf{v}_{e1}^*] + \frac{e}{c}[\mathbf{v}_{e1}^*\times\mathbf{B}_1 + \mathbf{v}_{e1}\times\mathbf{B}_1^*] \right\} \tag{3}$$

for the static nonlinear response (ponderomotive force[18,19]), where an asterisk denotes complex conjugate quantities. Using the set of conventional cylindrical coordintes (r,ϕ,z) and noting that in a linear approximation $\mathbf{B}_1 = (B_{r1}, 0, B_{z1})$, $\mathbf{E}_1 = (0, E_{\phi 1}, 0)$, $\mathbf{v}_{e1} = (0, v_{e\phi 1}, 0)$,[17] we obtain

$$F_{\mathrm{NLz}}^{2\omega} = \frac{e}{4c} v_{e\phi 1} B_{r1}$$

and

$$F_{\mathrm{NLr}}^{2\omega} = \frac{m_e}{4}\left[\frac{v_{e\phi 1}^2}{r} + \frac{e}{m_e c} v_{e\phi 1} B_{z1} \right]$$

for the axial and radial components of the second-harmonic nonlinear force. It is notable that there is no nonlinear force acting on the plasma electrons in the azimuthal direction $(\mathbf{F}_{\mathrm{NL}\phi}^{2\omega} = 0)$. Thus, the nonlinear second-harmonic currents are indeed driven in the poloidal $(r-z)$ cross section.

The components of the nonlinear second-harmonic force can be calculated using the following expressions for the linear electromagnetic fields in the cylindrical metal chamber of radius R and length L sealed at its top by a dielectric window with dielectric constant ε_d approximating the real vacuum vessel of our experiments,

$$B_{z1} = A\sum_{n=1}^{\infty} \frac{\alpha_{1n}\kappa_n^H}{D_n(TE)} \zeta_n^H(z) J_0(\kappa_n^H r), \tag{4}$$

$$B_{r1}^p = A\sum_{n=1}^{\infty} \frac{\alpha_{1n}\gamma_n^H}{D_n(TE)} \eta_n^H(z) J_1(\kappa_n^H r), \tag{5}$$

and

$$E_{\phi 1}^p = i\frac{\omega}{c} A\sum_{n=1}^{\infty} \frac{\alpha_{1n}}{D_n(TE)} \zeta_n^H(z) J_1(\kappa_n^H r), \tag{6}$$

$$v_{e\phi 1} = -i\frac{e}{m_e(\omega + i\nu_e)} E_{\phi 1}, \tag{7}$$

where

$$\zeta_n^H(z) = \sinh[\gamma_n^H(L-z)]/\cosh(\Gamma_n^H d)\cosh(\gamma_n^H L),$$

$$\eta_n^H(z) = \cosh[\gamma_n^H(L-z)]/\cosh(\Gamma_n^H d)\cosh(\gamma_n^H L),$$

$$D_n(TE) = \Gamma_n^H \coth(\Gamma_n^H d) + \gamma_n^H \coth(\gamma_n^H L),$$

$$\alpha_{1n} = [8\pi/cR^2 J_2^2(\rho_{1n})] \int_0^R r J_1(\kappa_n r)\, dr,$$

ϕ is the azimuthal angle, $\Gamma_n^H=[(\kappa_n^H)^2-(\omega/c)^2\varepsilon_d]^{1/2}$ and $\gamma_n^H=[(\kappa_n^H)^2-(\omega/c)^2\varepsilon_p]^{1/2}$ are the inverse rf field penetration lengths into dielectric and plasma, respectively.[12] Furthermore, we have $J_j(x)$ is a Bessel function of the jth order, $J_1(\rho_{1n})=0$, $\kappa_n^H=\rho_{1n}/R$, $\varepsilon_p=1-\omega_{pe}^2/[\omega(\omega+i\nu_e)]$ is the dielectric constant of the uniform plasma, and ω_{pe} is the electron Langmuir frequency. In the above, the azimuthal symmetry of the problem ($\partial/\partial\phi=0$) was assumed as well.

Solving the set of Maxwellian equations with relevant nonlinear terms, we arrive at the following nonlinear equation for the nonlinear azimuthal magnetic field at the second Fourier harmonic:

$$\frac{\partial}{\partial r}\frac{1}{r}\frac{\partial}{\partial r}(rB_{\phi 2})+\frac{\partial^2 B_{\phi 2}}{\partial z^2}+\frac{4\omega^2}{c^2}\varepsilon_{2\omega}B_{\phi 2}=i\frac{2\omega\chi_{2\omega}}{ce}\left[\frac{\partial F_{\mathrm{NLr}}^{2\omega}}{\partial z}-\frac{\partial F_{\mathrm{NLz}}^{2\omega}}{\partial r}\right], \tag{8}$$

where $\varepsilon_{2\omega}=1-\chi_{2\omega}$ and $\chi_{2\omega}=\omega_{pe}^2/2\omega(2\omega+i\nu_e)$. The nonlinear signal at the second harmonic also includes the radial

$$E_{r2}=-\frac{ic}{2\omega\varepsilon_{2\omega}}\frac{\partial B_{\phi 2}}{\partial z}-\frac{\chi_{2\omega}}{e\varepsilon_{2\omega}}F_{\mathrm{NLr}}^{2\omega}$$

and axial

$$E_{z2}=\frac{ic}{2\omega\varepsilon_{2\omega}}\frac{1}{r}\frac{\partial}{\partial r}(rB_{\phi 2})-\frac{\chi_{2\omega}}{e\varepsilon_{2\omega}}F_{\mathrm{NLz}}^{2\omega}$$

components of the electric field. Other components of the electromagnetic field do not feature the second harmonic terms. In the approximation adopted here, the nonlinear poloidal current at the second harmonic can be calculated as

$$\mathbf{j}_{\mathrm{pol}}^{2\omega}=\mathbf{r}j_r^{2\omega}+\mathbf{z}j_z^{2\omega},$$

where $j_{(r,z)}^{2\omega}=\sigma E_{(r,z)2}$, $\sigma=\omega_{pe}^2/4\pi(\nu_e-i\omega)$ is the conductivity of the uiniform collisional plasma. Here, $\mathbf{r}$ and $\mathbf{z}$ are the unit vectors in radial and axial directions, respectively.

IV. DISCUSSION

Thus, the nonlinear second-harmonic terms appear as a result of nonlinear interactions between the linear azimuthal current $j_{\phi 1}^{\omega}$ with the linear magnetic fields B_{r1} and B_{z1}. This interaction leads to pronounced generation of the poloidal second harmonic rf currents that in turn self-consistently generate the nonlinear magnetic field at the second Fourier harmonics $B_{\phi 2}^{2\omega}$ detected in our experiments. However, one should exercise a certain degree of caution in using our model for direct comparison of the theoretical and experimental data due to its semiqualitative character. The qualitative comparison of the nondimensional solution $\mathcal{B}_{\phi 2}=B_{\phi 2}(\kappa_1^H)^2/\beta_1$ of Eq. (8) with the experimental data is displayed in Fig. 6. Here, the normalized radial distance is $\kappa_1^H r$, $\beta_1=-ie\omega\chi_{2\omega}\gamma_1^{H,\omega}A^2/2c^3m_e(\omega+i\nu_e)\kappa_1^H$, and $\gamma_1^{H,2\omega}\approx 2\gamma_1^{H,\omega}$. One can note that even though the theoretical results fairly correctly describe the general tendencies in the radial profile of the azimuthal magnetic field at the second harmonic, the maximum theoretical and experimental values of the $B_{\phi 2}$ signal at 2ω are shifted a few centimeters apart from each other.

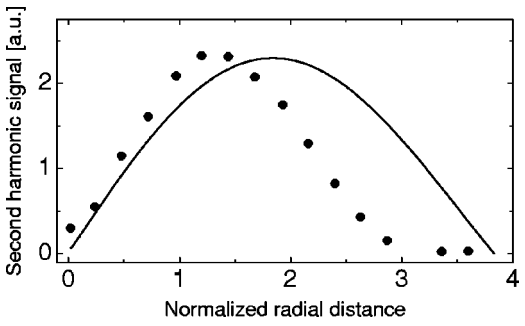

FIG. 6. Comparison of the computed (solid curve) radial profile of the normalized azimuthal magnetic field $\mathcal{B}_{\phi}^{2\omega}$ with the corresponding experimental profile of Fig. 4 for $\gamma_1^{H,2\omega}/\kappa_1^H\approx 1.1$.

One of the possible reasons for the apparent discrepancy is the limitation of the weak nonlinearity approach adopted here. Indeed, since the nonlinear second harmonic signal $B_{\phi}^{2\omega}$ at higher powers can in several times larger the corresponding linear component B_{ϕ}^{ω}, the weak nonlinearity approximation used here can eventually become invalid. This is illustrated in Fig. 7, where the nonlinear-to-total signal ratio $\vartheta=B_{\phi}^{2\omega}/[(B_z^{\omega})^2+(B_r^{\omega})^2+(B_{\phi}^{2\omega})^2]^{1/2}$ is plotted for the experimental parameters of Fig. 4. The above ratio does reflect the strength of the plasma nonlinearities in the electromagnetic mode of the low-frequency inductively coupled discharges. From Fig. 7, it is clearly seen that the nonlinear magnetic field at the second harmonic is significant at radial distances $2<r<10$ cm. Accordingly, the series expansion of the total nonlinear signal into higher harmonics with the amplitudes $A_{j+1}\ll A_j$, which was used to derive Eq. (8) remains fairly accurate except for the radial area $2<r<7$ cm, where the nonlinear parameter ϑ exceeds 0.2, a qualitative marginal parameter for the weak nonlinearity approximation to remain valid.[20]

Moreover, the simple fluid model adopted in this study assumes the axial and radial uniformity of the plasma density and electron temperature. In reality, assumption $T_e=\mathrm{const}(r,z)$ is usually justified better than $n_e=\mathrm{const}(r,z)$. For the electron number density, a flattened in the central areas ($r<8-10$ cm in the chamber with $R=16$ cm) of the moderate-power H-mode discharge and declining towards the walls radial profiles are more realistic[17] even though they deviate from conventional Bessel-type profiles presumably due to ponderomotive effects.[12] Radially, the plasma density

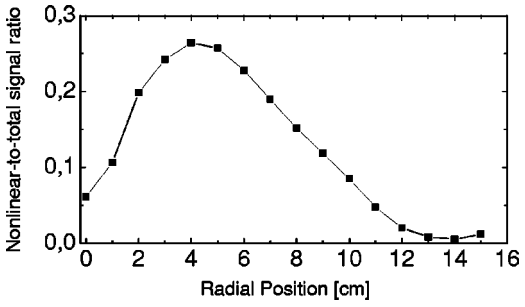

FIG. 7. Radial dependence of the nonlinear-to-total magnetic field signal ratio for the parameters of Fig. 4.

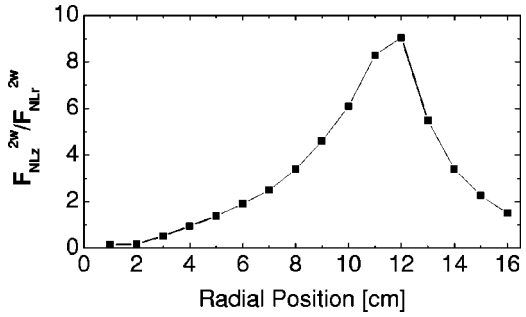

FIG. 8. Ratio of the azimuthal and radial second-harmonic components of the nonlinear Lorentz force vs radial distance for the parameters of Fig. 4.

is typically distributed cosinewise with the minima near the chamber bottom endplate and the dielectric window.[15] Thus, the nonlinearities of Sec. III can be considered fairly accurate in the central areas of the plasma glow (approximately $r<8-10$ cm and $5<z<15$ cm). Nevertheless, the model in question does correctly predict generation of poloidal rf currents and azimuthal magnetic field at the second Fourier harmonics and can be used for qualitative explanation of the observed effect.

The nonuniformities of the electron number density can become important and the corresponding nonlinear terms can appear in the form of so-called ''electron nonlinearities,'' with the second and third order nonlinear responses calculated for unmagnetized low-temperature plasmas in Refs. 21 and 22. Likewise, the effect of steady magnetic fields on the plasma nonlinearities is discussed elsewhere.[22]

It is worthwhile to mention that the direction of the resulting nonlinear force $\mathbf{F}_{\mathrm{NL}}^{2\omega}=\mathbf{r}F_{\mathrm{NLr}}^{2\omega}+\mathbf{z}F_{\mathrm{NLz}}^{2\omega}$ appears to change at different radii. Figure 8 illustrates the variation of the ratio of the axial and radial components of the nonlinear force $F_{\mathrm{NLz}}^{2\omega}/F_{\mathrm{NLr}}^{2\omega}$ along the chamber radius. From Fig. 8 one can deduce that for the experimental parameters of Fig. 4 the azimuthal component of the nonlinear Lorentz force is always larger than the radial one. Furthermore, one can conclude that for radial positions $10<r<13$ cm the resulting nonlinear force $\mathbf{F}_{\mathrm{NL}}^{2\omega}$ is directed along the chamber axis. In this case the radial component turns out to be 6–9 times less than the axial one.

Meanwhile, one can expect that in nonuniform plasmas $[n_e\neq\mathrm{const}(r,z)]$ the nonlinear second-harmonic force at the second Fourier harmonic $F_{\mathrm{NL}\phi}^{2\omega}$ becomes nonvanishing due to the electron nonlinearities. Physically, the azimuthal component of the second harmonic nonlinear force can be used as an indicator of the importance of nonuniformities in the electron number density in generating the nonlinear plasma response. Thus, proper diagnostics of $F_{\mathrm{NL}\phi}^{2\omega}$ can be instrumental in assessing the nonlinear behavior of the inductively coupled plasmas with certain electron/ion density profiles.

It is remarkable that the nonlinear radial second-harmonic force $\mathbf{F}_{\mathrm{NLr}}^{2\omega}$ contains contributions from the nonlinear Lorentz force ($\sim v_{e\phi 1}B_{z1}$) and nonlinear (also nonuniform) electric field $\sim v_{e\phi 1}^2/r$. However, the estimates show that for the typical parameters of our experiments in the electromagnetic discharge regime, the contribution of the latter term is 1–2 orders of magnitude smaller and can be neglected.

Finally, due to apparent similarity in the procedure of derivation of the ponderomotive force-caused nonlinear terms, one can also expect pronounced generation of the nonlinear static azimuthal magnetic field $B_{\phi 2}^{(0)}$. Thus, future research into modeling and experimental verification of the nonlinear static responses in low-frequency inductively coupled plasmas is warranted.

ACKNOWLEDGMENTS

This work was supported in part by the Australian Research Council, Agency for Science, Technology, and Research of Singapore (Project No. 012-101-00247) and the Flinders Institute for Research in Science and Technology.

[1] H. Sugai, T. H. Ahn, I. Ghanashev, M. Goto, M. Nagatsu, K. Nakamura, K. Suzuki, and H. Toyoda, Plasma Phys. Controlled Fusion **39**, A445 (1997).
[2] L. Delzeit, I. McAninch, B. A. Cruden, D. Hash, B. Chen, J. Han, and M. Meyyappan, J. Appl. Phys. **91**, 6027 (2002).
[3] M. Tuszewski, Phys. Plasmas **5**, 1198 (1998).
[4] H. Sugai, K. Nakamura, and K. Suzuki, Jpn. J. Appl. Phys., Part 1 **33**, 2189 (1994).
[5] K. Suzuki, K. Nakamura, H. Ohkubo, and H. Sugai, Plasma Sources Sci. Technol. **7**, 13 (1998).
[6] M. Tuszewski, IEEE Trans. Plasma Sci. **27**, 68 (1999).
[7] L. Stenflo and M. Y. Yu, Nature (London) **384**, 224 (1996).
[8] L. Stenflo and M. Y. Yu, Phys. Plasmas **5**, 3122 (1998); Phys. Rev. A **42**, 4894 (1990).
[9] C. M. Ryu and M. Y. Yu, Phys. Scr. **57**, 601 (1998).
[10] S. V. Vladimirov, V. N. Tsytovich, and M. Y. Yu, Phys. Rep. **241**, 1 (1994).
[11] N. F. Cramer, J. Phys. D **30**, 2573 (1997); T. A. van der Straaten, N. F. Cramer, I. S. Falconer, and B. W. James, *ibid.* **31**, 191 (1998).
[12] S. Xu, K. N. Ostrikov, W. Luo, and S. Lee, J. Vac. Sci. Technol. A **18**, 2185 (2000).
[13] S. Xu, K. N. Ostrikov, Y. Li, E. L. Tsakadze, and I. R. Jones, Phys. Plasmas **8**, 2549 (2001).
[14] K. N. Ostrikov, S. Xu, and A. B. M. Shafiul Azam, J. Vac. Sci. Technol. A **20**, 251 (2002).
[15] M. A. Lieberman and A. J. Lichtenberg, *Principles of Plasma Discharges and Materials Processing* (Wiley, New York, 1994).
[16] I. M. El-Fayoumi and I. R. Jones, Plasma Sources Sci. Technol. **7**, 162 (1998).
[17] K. N. Ostrikov, I. B. Denysenko, E. L. Tsakadze, S. Xu, and R. G. Storer, J. Appl. Phys. **92**, 4935 (2002).
[18] S. V. Vladimirov, Phys. Lett. A **219**, 233 (1996).
[19] R. B. Piejak and V. A. Godyak, Appl. Phys. Lett. **76**, 2188 (2000).
[20] N. A. Azarenkov and K. N. Ostrikov, Phys. Rep. **308**, 333 (1999).
[21] S. V. Vladimirov and V. N. Tsytovich, Sov. J. Plasma Phys. **14**, 349 (1988) [Fiz. Plazmy **14**, 593 (1988)].
[22] S. V. Vladimirov, V. N. Tsytovich, S. I. Popel, and F. Kh. Khakimov, *Modulational Interactions in Plasmas* (Kluwer Academic, Dordrecht, 1995).